1 # *In situ* Transmission Electron Microscopy Observation of Melted
2 Germanium Encapsulated in Multilayer Graphene

3 **Seiya Suzuki[1-3,*], Yoshihiro Nemoto[4], Natsumi Shiiki[2], Yoshiko Nakayama[4], and Masaki Takeguchi[4]**

4 [1]Advanced Science Research Center (ASRC), Japan Atomic Energy Agency (JAEA), 2-4 Shirakata, Tokai,
5 Ibaraki 319-1195, Japan
6 [2]International Center for Young Scientists (ICYS), National Institute for Materials Science (NIMS), 1-1
7 Namiki, Tsukuba, Ibaraki 305-0044, Japan
8 [3]PRESTO, Japan Science and Technology Agency (JST), 4-1-8 Honcho, Kawaguchi, Saitama 332-0012,
9 Japan.
10 [4]Electron Microscopy Analysis Station, National Institute for Materials Science（NIMS), 1-2-1 Sengen,
11 Tsukuba, Ibaraki 305-0047, Japan
12 [*]suzuki.seiya35@jaea.go.jp and seiya09417@gmail.com
13

14 **ABSTRACT**

15 Germanene is a two-dimensional (2D) germanium (Ge) analogous of graphene, and its unique topological
16 properties are expected to be a material for next-generation electronics. However, no germanene
17 electronic devices have yet been reported. One of the reasons for this is that germanene is easily oxidized
18 in air due to its lack of chemical stability. Therefore, growing germanene at solid interfaces where it is
19 not oxidized is one of the key ideas for realizing electronic devices based on germanene. In this study,
20 the behavior of Ge at the solid interface at high temperatures was observed by transmission electron
21 microscopy (TEM). To achieve such *in situ* heating TEM observation, we fabricated a
22 graphene/Ge/graphene encapsulated structure. *In situ* heating TEM experiments revealed that Ge like
23 droplets moved and coalesced with other Ge droplets, indicating that Ge remained as a liquid phase
24 between graphene layers at temperatures higher than the Ge melting point. It was also observed that
25 droplet Ge incorporates the surrounding amorphous Ge as Ge nuclei, thereby increasing its size (domain

26 growth). These results indicated that Ge crystals can be grown at the interface of van der Waals materials,
27 which will be important for future germanene growth at solid interfaces.

28

29 **Introduction**

30 Germanene is a two-dimensional (2D) germanium (Ge) analogous to graphene.[1] Theoretical studies have
31 predicted that germanene has linear band dispersion,[1-2] a size-tunable band gap by applying an electric
32 field,[3] and topological properties.[1, 4] Owing to those unique physical properties, electronic device
33 applications of germanene, such as field effect transistors (FETs),[5] has been highly demanded as well as
34 silicene,[2, 6] stanene,[7] and plumbene.[8] Nevertheless the growth of germanene has already been reported
35 on various surfaces, such as Ag(111),[9] Au(111),[10] Cu(111),[11] Al(111),[12] Pt(111),[13] graphite,[14] and
36 MoS_2,[15] the electronic devices of germanene have not been reported yet. Even though by taking into
37 account other the related group-14 2D monoatomic layers, the reports of their electronic devices are
38 limited except the hydrogenated germanene (germanane)[16] and silicene FETs.[17] One of the reasons for
39 this is chemical instability of group-14 based 2D monoatomic layers including germanene. Once high-
40 quality germanene is grown on a surface in an ultra-high vacuum chamber, but it is easily degraded by
41 oxidation in air. Thus, the fabrication of electronic devices of germanene and other group-14 2D
42 monoatomic layers is difficult, in contrast to chemically stable 2D materials, such as graphene and
43 transition metal dichalcogenides (TMD).

44 As one approach, we have come up with the idea of growing germanene directly at the solid interface,
45 where it is not oxidized in air.[9f] Based on this concept, we have grown germanene at the interfaces of
46 graphene/Ag(111) and hexagonal boron nitride (hBN)/Ag(111).[9a] This work proved that the high gas
47 barrier properties of graphene and hBN allow the germanene at such interfaces to be stable in air. However,

this growth method still remains challenges for the fabrication of germanene devices since the germanene is not electrically isolated due to the contacting Ag surface. This is a common challenge for germanene grown on metal surfaces. In order to realize germanene FETs from growing it on a metal surface, the physical or electrical separation of germanene from the grown metal surface will be required.

On the other hand, if germanene can be formed directly at the interface of insulators, the issue of contact between germanene and metal surfaces does not arise, and the development of germanene devices should be achieved. To maximize the potential of germanene, hBN would be a very promising encapsulation material among insulators. The advantages of hBN encapsulation are that it provides an atomically smooth surface (or interface), free of dangling bonds, and screening substrate effects such as scattering for preserving (modulating, or enhancing) the intrinsic properties of the encapsulated 2D monatomic layer. These have already been well demonstrated in the carrier transport measurements of graphene[18] and TMD.[19]

The direct growth of germanene between hBN layers, as well as the growth of other group 14 monoatomic 2D materials, has not been achieved to date. In order to form germanene between 2D materials, we need to insert Ge sources and crystalize them. Crystal growth from molten state (Czochralski method)[20] and phase transition from amorphous state[21] are typical ways to form bulk and crystalline thin films of Ge, respectively, and we thought that employing these methods would be a reasonable way to challenge the growth of germanene between 2D materials. In this study, we fabricated a Ge encapsulated structure with graphene layers and observed the behavior of the encapsulated Ge at high temperatures using *in situ* heating transmission electron microscopy (TEM). Graphene, which produces van der Waals (vdW) interfaces similar to those of hBN, was used as an alternative material to hBN. From the TEM observation, we found that Ge between graphene were able to exist at more than the melting point of Ge (MP_{Ge}), indicating that the graphene layers successfully encapsulate the Ge layer. After several heating processes,

71 amorphous Ge and crystalline Ge coexisted between the graphene layers. The shape of crystalline Ge is
72 almost spherical (named droplet Ge), indicating three-dimensional nucleation. At higher temperatures
73 than MP_{Ge}, the movement of Ge droplets and their coalescence with other Ge droplets in the surrounding
74 area were observed. Atomic resolution TEM observations showed that some droplets were liquid at high
75 temperatures because they did not have clear lattice fringes. Since crystalline Ge particles were observed
76 at room temperature (RT), the droplets crystallized when they cooled down. Our observations suggest
77 that it is important to avoid the formation of droplet when growing planar Ge crystals (germanene)
78 between vdW materials, which can provide hints for the direct growth of germanene at solid interfaces in
79 the future.

80

81 **Results and Discussion**

82 **1. Preparation and observation of graphene/Ge/graphene encapsulated structure**

83 Figure 1 shows the sample preparation of encapsulated Ge between graphene layers for *in situ* heating
84 TEM observation. The sample preparation consists of chemical vapor deposition (CVD) growth of
85 graphene, transfer graphene, Ge deposition, and encapsulation of Ge by graphene. CVD growth was done
86 onto a commercial copper (Cu) foil by using a homemade CVD furnace. The grown graphene is
87 polycrystalline and has a high surface coverage. Figure 1(a) illustrates a transfer process of monolayer-
88 graphene (1L-graphene) onto another CVD graphene/Cu. The grown graphene/Cu (1) was first spin-
89 coated by poly(methyl methacrylate) (PMMA) as a mechanical support layer (2). After drying, the Cu
90 substrate was etched away with metal etchant (3) followed by multiple deionized (DI) water rinses (4).
91 The PMMA/graphene was then scooped up with another graphene/Cu (5), and finally the PMMA layer
92 was removed with acetone (6). This graphene transfer was repeated to fabricate 4L-graphene. Figure 1(b)
93 shows the encapsulation of Ge by graphene and the transfer of the encapsulated Ge onto a Nano-Chip

94 (Wildfire, DENSsolutions) designed for *in situ* heating TEM observation. A 4L-graphene/Cu (7) and a
95 Ge thin film deposited 4L-graphene/Cu (8) were prepared for the Ge encapsulation. The Ge thin film was
96 patterned using a metal shadow mask during the electron beam deposition of Ge. By patterning Ge, the
97 contact area between the top and bottom 4L-graphene is increased, which improves their adhesion. The
98 transfer of the 4L-graphene onto the Ge/4L-graphene/Cu was also performed in the same way (9,10) as
99 the transfer process in Fig. 1(a). Finally, the 4L-graphene/Ge/4L-graphene was transferred by scooping
100 up with a Nano-Chip (11).

101 We also tried to encapsulate Ge with two sheets of 1L-graphene, but the Ge disappeared after metal
102 etching. This is probably due to the metal etchant permeation into Ge across the graphene, indicating the
103 imperfections in graphene, such as defects, grain boundaries, wrinkles, insufficient adhesion to Ge, and
104 their occurrence during the transfer process. By increasing the number of graphene layers, the loss of Ge
105 was strongly suppressed, and 4Ls were found to be thick enough to fabricate a graphene/Ge/graphene
106 encapsulation structure.

107

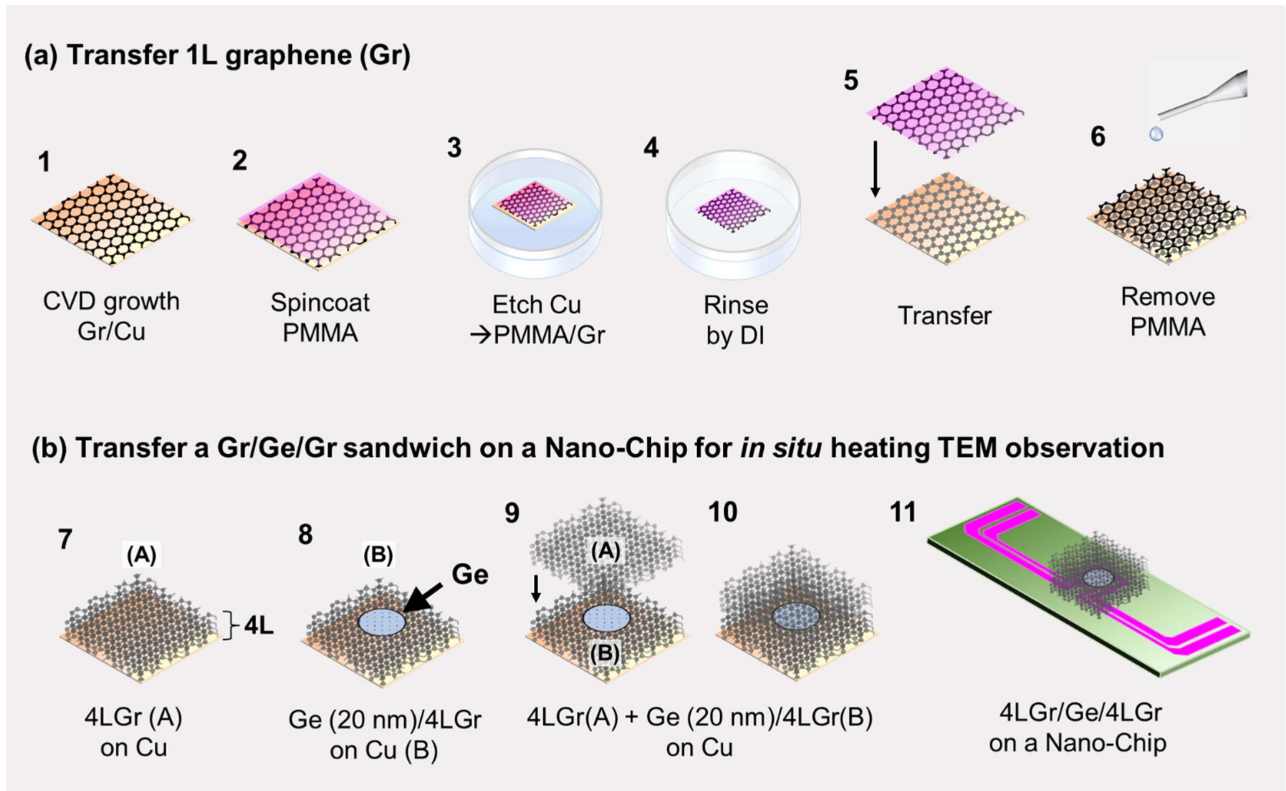

108 **Figure 1.** Sample preparation of encapsulated Ge between graphene layers onto a Nano-Chip (Wildfire,
109 DENSsolutions) designed for *in situ* heating TEM observation. (a) Transfer 1L-graphene onto 1L-
110 graphene/Cu for increasing the number of layers. (b) Encapsulation of Ge and transfer onto a Nano-Chip.

111

112 Figure 2(a) shows a photograph of the Nano-Chip. The size of the Nano-Chip is approximately 4 mm ×
113 10 mm. The graphene/Ge/graphene was placed inside the broken-line rectangular area where the heater
114 of the Nano-Chip is located. Figure 2(b) shows the SEM image of the heater part after the
115 graphene/Ge/graphene transfer. The heater has a spiral shape. Figure 2(c) shows a magnified SEM image
116 and the Raman spectrum recorded inside the lower hole (red arrow). In the Raman spectrum, D, G, and
117 G' (2D) peaks were observed at ~1360, ~1583, and 2725 cm^{-1}, respectively. The small intensity of the D
118 peak and the narrow bandwidth of the G peak (about 16 cm^{-1} at full width half maximum) indicate high

crystallinity.[22] The G'/G peak intensity ratio (~0.8) indicates multilayer graphene,[22b, 22c] which is consistent with our sample preparation process. Figure 2(d) shows the schematic cross-sectional view of the fabricated sample. Figure 2(e) shows an energy dispersive X-ray spectroscopy (EDS) spectrum obtained at the center of the lower hole (red arrow). Ge, Cu, oxygen (O), nitrogen (N), carbon (C), and silicon (Si) were detected. The detected Cu is the residue from the substrate of CVD graphene, and the Si and N are from the Nano-Chip. The detection of the Ge signal suggests that the sample preparation of the Ge encapsulation by graphene was successful.

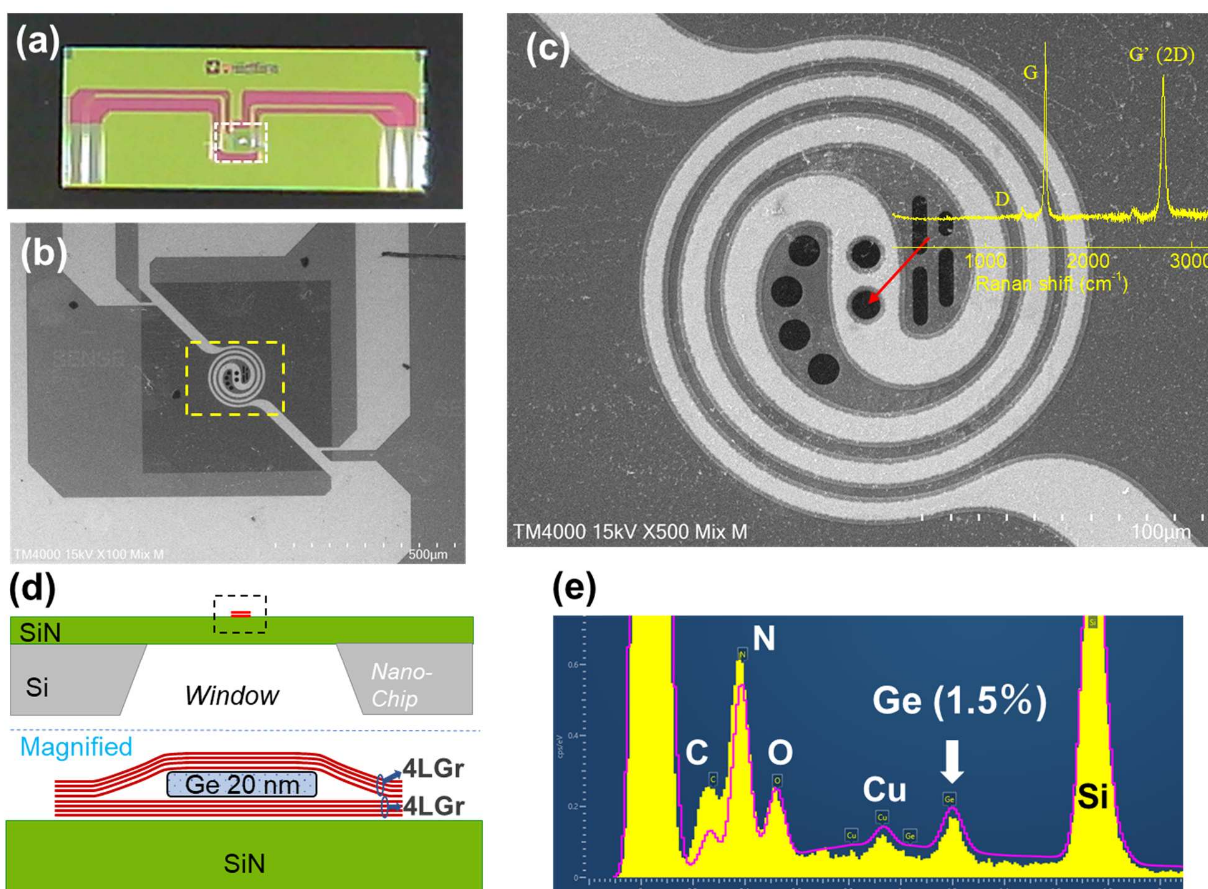

Figure 2. (a) Photograph of the Nano-Chip. (b) The SEM image of the heater part after the graphene/Ge/graphene transfer. (c) Magnified SEM image and the Raman spectrum recorded inside the

129 lower hole (red arrow). (d) Schematic cross-sectional views of the fabricated sample. (e) EDS spectrum
130 obtained at the center of the lower hole.

131

132 Figures 3(a) and 3(b) are high-angle annular dark field scanning TEM (HAADF-STEM) images of the
133 graphene/Ge/graphene sample at RT before and after EDS analysis, respectively. Figures 3(c-h) show the
134 EDS maps of C, N, O, Si, Cu, and Ge. The distributions of N, Si, and Cu were not clearly defined in the
135 EDS maps due to the very low abundance or uniform distribution of these elements. On the other hand,
136 the distribution of Ge was clearly detected by the EDS map (Fig. 3(h)). Since the signal obtained by
137 HAADF-STEM is proportional to the α power of the atomic number (Z) [Z^{α} ($\alpha = 1.3 \sim 2$)],[23] the bright
138 contrasts in Figs. 3(a) and (b) indicate Ge morphology. The observed Ge was agglomerated, which was
139 probably due to the insufficient adhesion between Ge and graphene. As can be seen in Figs. 3(a) and 3(b),
140 the morphology of Ge changes from lumpy to smoothly connected aggregates after long-time electron
141 beam irradiation (>1 hour) during the EDS mapping measurement. Although the detailed mechanism of
142 the morphological change is unclear, unnecessary electron beam irradiation was avoided in order to
143 minimize damage to the sample hereafter.

144

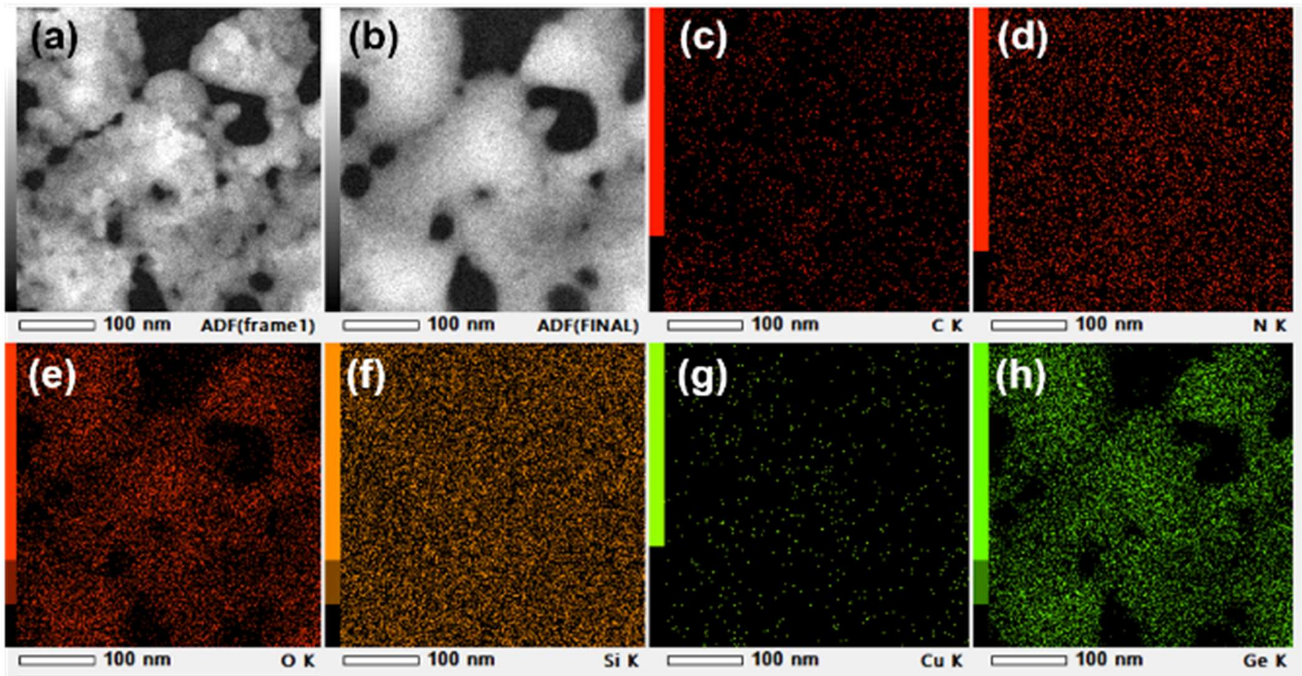

145 **Figure 3.** HAADF-STEM images and EDS maps of the graphene/Ge/graphene sample at RT before
146 annealing processes. HAADF-STEM images (a) before and (b) after EDS analysis. EDS maps of (c) C,
147 (d) N, (e) O, (f) Si, (g) Cu, and (h) Ge.

148

149

150 Subsequently, we started to heat the sample using the *in situ* heating holder followed by TEM observation.
151 The sample was annealed many times with simple heating profiles of different temperatures (T) and
152 heating time duration (t_{HT}) as shown in Fig. 4. The typical heating rate was approximately +100 °C/min
153 and typical cooling rate was approximately -100 °C/min. All annealing processes for this sample are
154 summarized in Table 1.

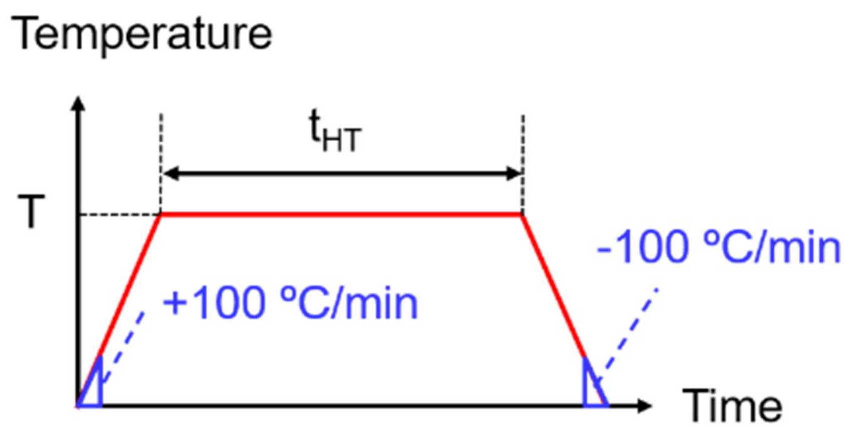

155

156 **Figure 4.** Schematic of the heating profile for the graphene/Ge/graphene sample for each annealing
157 process. t_{HT} is heating time duration.

158

159

160

161

162

163

164 **Table 1.** Heating temperature (T) and time (t_{HT}) for all annealing processes for the graphene(4L)/Ge(20
165 nm)/graphene(4L) sample in this study.

process #	T (°C)	t_{HT} (min)
1	RT	-
2	650	10
3	700	10
4	750	10
5	800	10
6	900	0.5
7	950	0.5
8	1000	0.5
9	1025	0.5
10	1050	0.5
11	1050	3
12	1025	0.5
13	1025	10
14	1050	20
15	1075	12
16	1075	10

166

167 To achieve the purpose of this study, we need to observe the crystallization of Ge between graphene layers
168 by TEM. However, the sample is not uniform as can be seen from Fig. 3. Therefore, we attempted to find
169 as complete a graphene/Ge/graphene region as possible for *in situ* observation. Figure 5(a) shows a TEM
170 image of the sample after annealing at 700 °C (process #3 in Table 1); the annealing at mild temperature
171 was performed to clean the sample. The band-like structure (from top left to bottom right) and dark
172 contrast in Fig. 5(a) are likely graphene and Ge, respectively. To determine the number of graphene layers,
173 HRTEM images and corresponding fast Fourier transform (FFT) images (Figs. 5(b-d)) were taken at the
174 arrowed points (b), (c), and (d) in Fig. 5(a). The FFT images (Figs. 5(b-d)) show several six-fold
175 symmetry spots corresponding to graphene. The transfer of graphene from one graphene to another
176 without intentional alignment in their crystalline direction, such as in the present sample preparation,
177 results in random stacking of those graphene layers at a high probability. Therefore, the number of six-

178 fold symmetry spots guarantees that the same number of graphene layers present at the point where the
179 FFT image were taken. Counting the number of spots in a 60-degree range in Figs. 5(b-d), 4, 7, and 8 six-
180 fold symmetry spots were observed, respectively, so that the numbers of graphene layers at these points
181 are 4, 7, and 8L. According to the numbers of those graphene layers at (b-d) and the TEM contrast in Fig.
182 5(a), the expected arrangement of graphene and Ge is shown in Fig. 5(e), where red (4L) and yellow (7-
183 8L) are being superimposed as the number of graphene layers on the TEM image (Fig. 5(a)). Since there
184 are a lot of dark contrast in the yellow region in Fig. 5(e), it is expected that graphene/Ge/graphene is
185 locally remaining. Figure 5(f) shows a possible cross-sectional structure on the line of α to β in Fig. 5(a).
186 Although it is possible that the Ge is not covered by graphene layers, as shown in Fig. 5(g), uncovered
187 Ge would evaporate at temperatures higher than MP_{Ge} (938°C) because of vapor pressure.

188

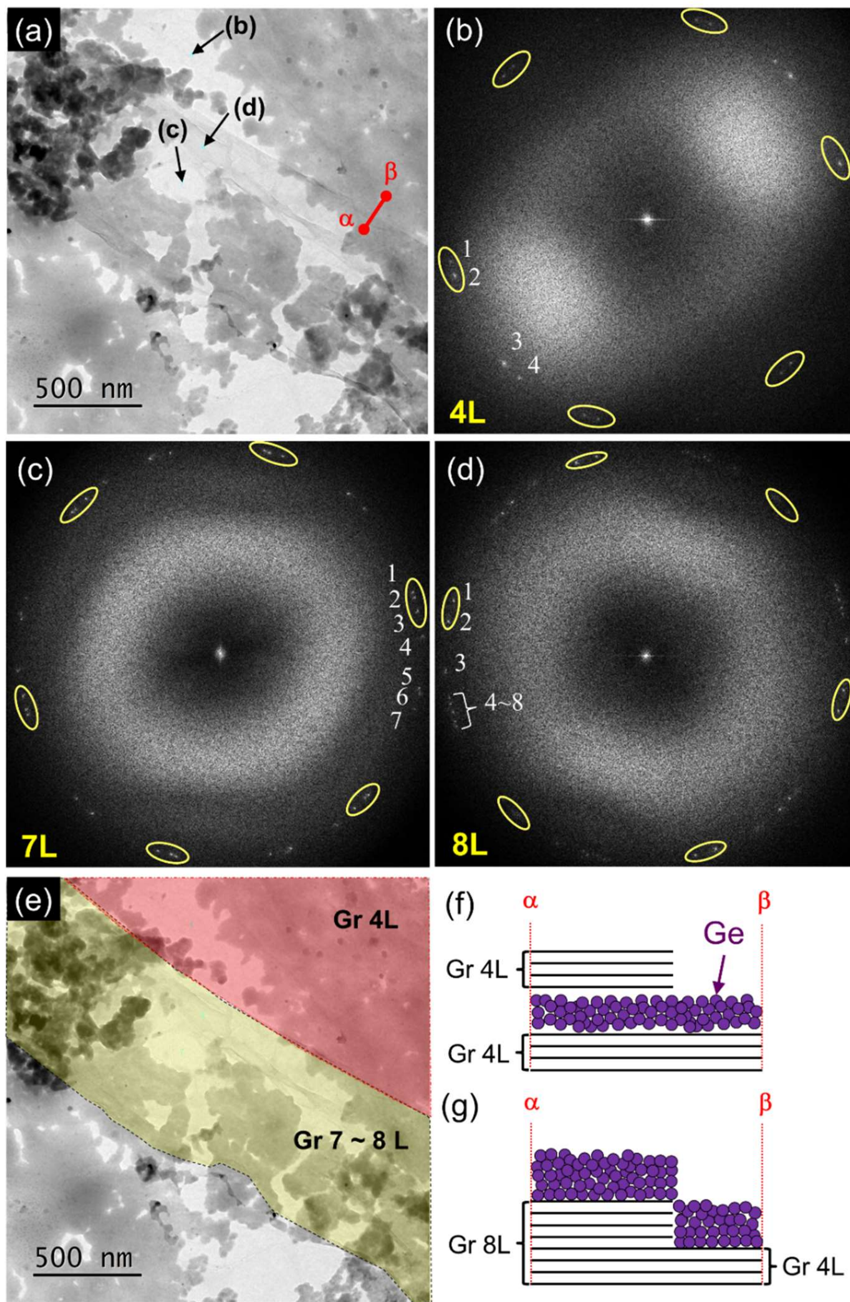

189 **Figure 5.** (a) TEM image of the sample after annealing at 700 °C (process #3). (b-d) FFT images obtained
190 in (a). The relatively clear 6-fold spots corresponding to graphene are encircled by ellipses as eye guides.
191 The white numbers indicate the numbers of spots counted in a 60-degree range. (e) Expected arrangement
192 of graphene and Ge. Red (4L) and yellow (7-8L) colors are superimposed as the number of graphene
193 layers on (a). (f,g) Possible cross-sectional structure on the line of α to β in (a).

194

195 **2. Suppression of Ge evaporation by graphene encapsulation**

196 To confirm the encapsulation of Ge by graphene layers, we performed several heating processes (#4 ~
197 12) including the heating temperatures higher than MP_{Ge}. Figures 6(a) and 6(b) show TEM images
198 obtained at RT after the annealing #12. The band-like structure expected to be a graphene/Ge/graphene
199 region seems to still present. Subsequently, additional annealing was performed at 1025 °C for 10 min
200 (process #13), and TEM observation was performed at RT in the exact same area as in Figs. 6(a) and 6(b).
201 Figures 6(c) and 6(d) show the TEM images after annealing at 1025 °C (process #13). It was observed
202 that the different contrast changes depending on the region by the annealing at 1025 °C. While the dark
203 contrasts were maintained or darkened more between the dashed lines in Fig. 7(c), the dark contrasts
204 disappeared or faded in the other regions. This indicates that graphene/Ge/graphene area exists between
205 the broken lines and that graphene encapsulation suppresses Ge evaporation at higher temperatures than
206 the MP_{Ge}. In the graphene-encapsulated regions, it was also observed that the number of black dots
207 increased and became more clearly visible. Figure 6(e) shows a HRTEM image of a black dot. Several
208 lattice fringes were observed in the HRTEM image. Figures 6(f) and 6(g) show the FFT images obtained
209 within the upper and lower circles enclosed by the yellow broken lines in Fig. 6(e), respectively. The FFT
210 images agree well with Ge (111) and Ge (110), indicating that the black dots are crystalline particles of
211 Ge. On the other hand, the majority of the surrounding area showed no spots in the FFT image. This
212 indicates that the majority of Ge between graphene layers remains amorphous state even after annealing
213 above MP_{Ge}.

214

215

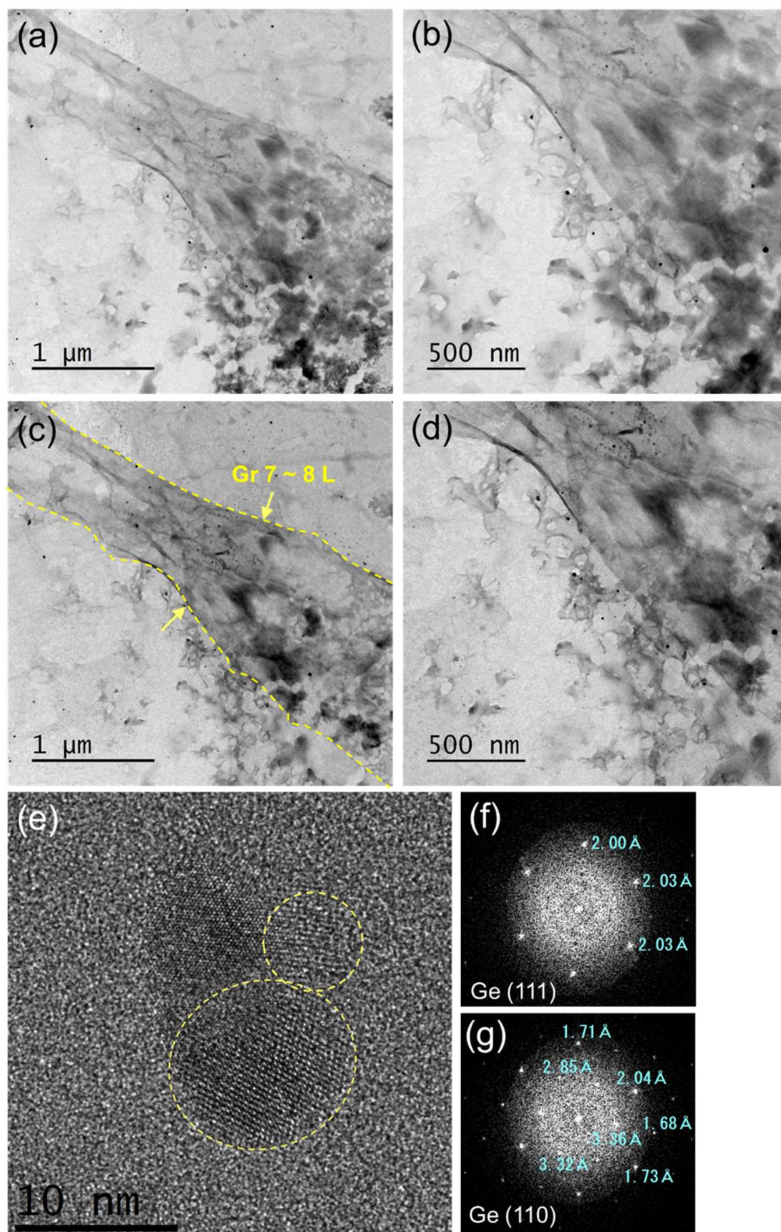

216 **Figure 6.** (a,b) TEM images obtained at RT after several heating processes (#4 ~ 12). (c,d) TEM images
217 obtained at the same area as in (a) and (b) after annealing at 1025 °C for 10 min (process #13). Expected
218 graphene covered region is between the broken yellow lines in (c). (e) HRTEM image of a black dot. (f,g)
219 FFT images obtained within the upper and lower circles enclosed by the yellow broken lines in (e),
220 respectively. The FFT images agree well with Ge (111) and Ge (110), indicating that the black dots are
221 crystalline Ge.

3. Crystal phase of Ge at high temperatures

Figure 7 shows the TEM images of black dots at high temperatures (>MP_{Ge}) extracted from the movie (S1 “fusion”) obtained by *in situ* TEM observation at 1050 °C (process #14). The time shown in the upper right corner for each TEM image correspond to the time after the start of the video (S1 “fusion”) recording in real time (The video plays at ~5x speed). We observed several spherical dark contrasts, which we will refer to hereafter as "droplet Ge". In Fig. 7, we mainly focused on the droplet Ge indicated by the arrow in the first TEM image (20s). As can be seen, the droplet Ge moved, deformed, and finally merged with the other droplet Ge on the right side. This flexible movement and coalescence of Ge indicates that the droplet Ge is in a liquid state at 1050 °C. It is noted that bare Ge (not covered by graphene) is not expected to exist in a liquid or solid state at 1050 °C, since the vapor pressure of Ge at 1050 °C is about 10 Pa, much higher than the pressure in the TEM chamber (< 2×10^{-5} Pa). On the other hand, the droplets showed a crystalline structure at RT (Figs. 6(e-g)), suggesting that they crystallized during cooling.

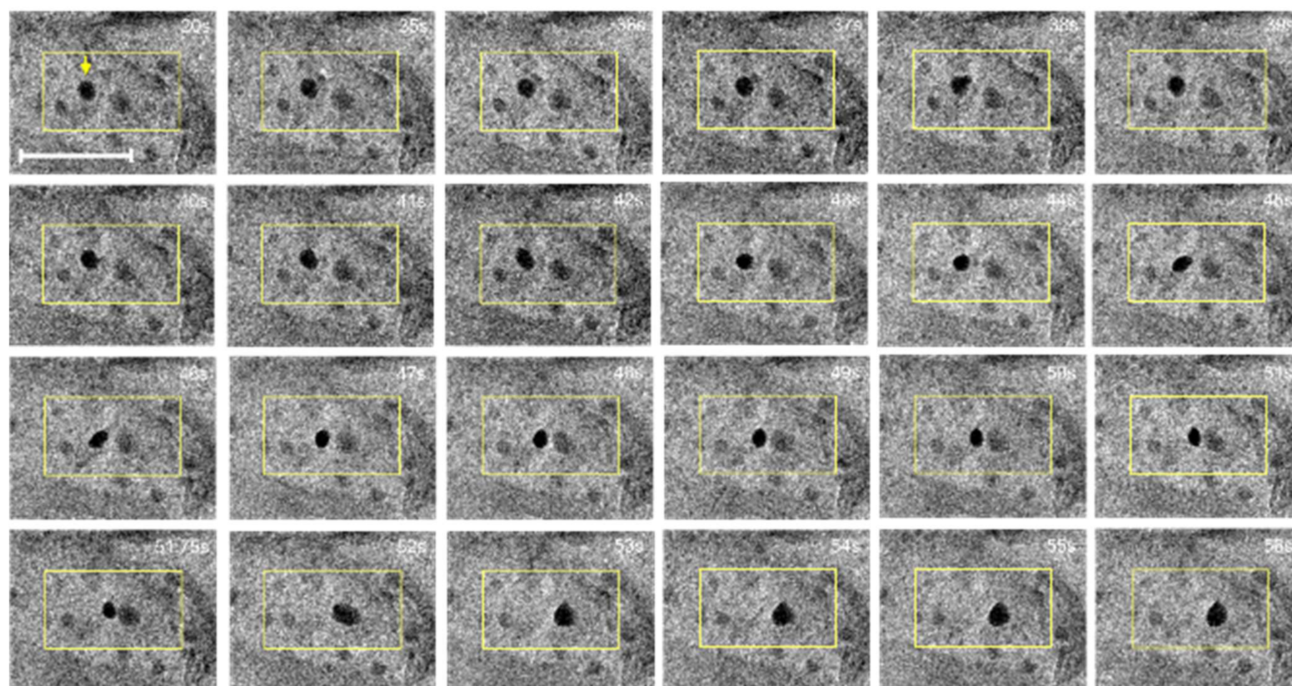

236 **Figure 7.** TEM images of black dots at high temperatures (>MP_{Ge}) extracted from the movie (S1 "fusion")
237 obtained by *in situ* TEM observation at 1050 °C. The times shown in the upper right corner for each TEM
238 image correspond to the time after the start of the video (S1 "fusion") recording in real time (not video
239 time).

240

241 Next, we performed HRTEM observation of droplet Ge at 1075 °C. Figure 8(a) shows an HRTEM image
242 extracted from the movie obtained by *in situ* TEM observation at 1075 °C (process #16). Figures 8(b-d)
243 show the FFT images in Fig. 8(a). We observed lattice fringes in the area shown in (b) of Fig. 8(a) (it is
244 more clearly seen in the area encircled by the ellipse in the lower center). The corresponding FFT image
245 (Fig. 8(b)) shows several spots, indicating the presence of ordered structure. On the other hand, some
246 droplets Ge do not have clear lattice fringes, such as (c) and (d) in Fig. 8(a). It is noted that the area (d)
247 may not be a droplet Ge but simply a vacant area. Those FFT images (Figs. 8(c) and 8(d)), which is
248 different from Fig. 8(b), shows a few faint and unclear spots. In addition, the obtained three FFT spot
249 patterns (Fig. 8(b-d)) do not agree with that of Ge (totally different from Figs. 6(f) and 6(g)), graphene,
250 or even meatal impurities such as Cu. We assumed that the observed FFT spot patterns are originated
251 from the structure of liquid Ge. It is widely reported that liquid Ge has short-range ordered structure.[24]
252 The reported average nearest-neighbor distances of Ge-Ge at high temperatures (2.66 Å at 1175-1650
253 K,[24b] 2.68-2.69 Å at 1120-1534 K,[24c] 2.74-2.76 Å at 1270-1870 K[24d]) are ~8% to ~13% larger than
254 crystalline Ge at RT (2.45-2.46 Å[24e]). Also, by taking into account the self-diffusion coefficient of Ge
255 atoms in liquid phase (1.3×10^{-8} m^2 s^{-1} at the temperature of MP_{Ge}[25]), Ge atoms in a droplet Ge move
256 extremely fast in the size of the HRTEM image. Therefore, the short-range ordered structure in liquid Ge
257 would result in different spot patterns in the FFT image as compared to diamond cubic crystal of Ge, and

258 the fast movement of Ge atoms in liquid Ge would cause fluctuations and instability in the FFT spot

259 patterns.

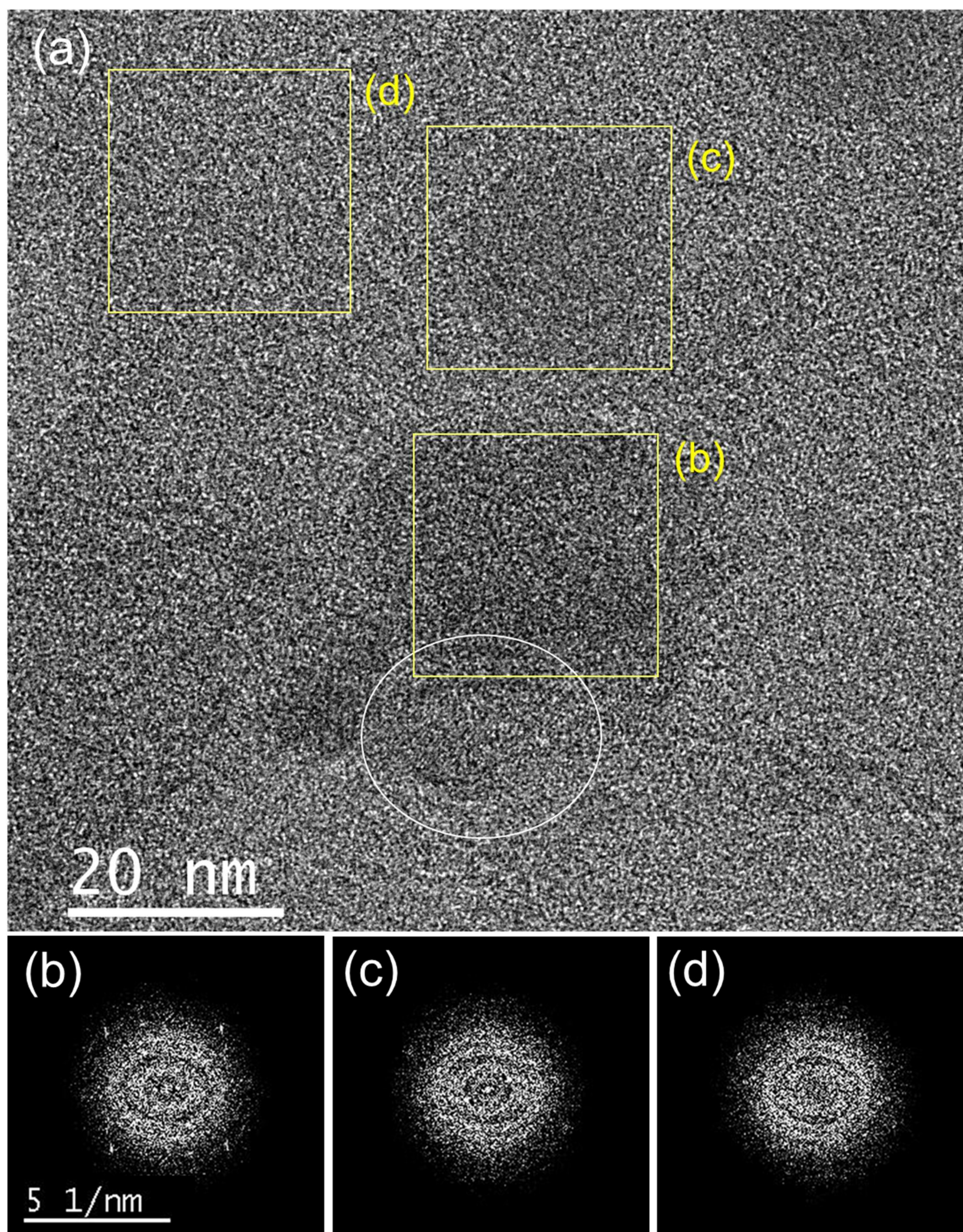

260

261 **Figure 8.** (a) HRTEM image of droplets Ge extracted from the movie obtained by *in situ* TEM observation

262 at 1075 °C (process #16). (b-d) FFT images obtained within (b), (c) and (d) in (a).

263

264 Figure 9 shows the STEM-EDS results obtained at RT after all annealing processes (after process #16).

265 Figure 9(a) shows the EDS spectrum. Figures 9(b) and 9(c) show HAADF-STEM images before and after

266 the EDS analysis, respectively. Figures 9(d-i) show EDS maps of C, N, O, Si, Cu, and Ge. From Fig. 9(a),

267 Ge and a little amount of Mo and Cu were detected. The Mo signal is from the material of heating wire

268 of the Nano-Chip. The Cu would be contamination from the sample preparation process (substrate of

269 graphene grown by CVD). Since the amount of Cu detected was very small and no agglomeration was

270 observed (Fig. 9(h)), it was confirmed that Cu did not affect the TEM observations and the

271 aforementioned discussion of droplet Ge. On the other hand, the contrast distribution in the HAADF-

272 STEM images (Figs. 9(b) and 9(c)) is consistent with the distribution of Ge (Fig. 9(i)). Thus, the particles

273 (droplet Ge) observed in Figs. 7 and 8 are surely made of Ge. Furthermore, no oxygen was detected at

274 the Ge positions (Fig. 9(f)), indicating that droplet Ge is pure germanium, not Ge oxides such as GeO_2.

275 These results suggest that Ge can exist as a liquid phase between vdW layers even above MP_{Ge}.

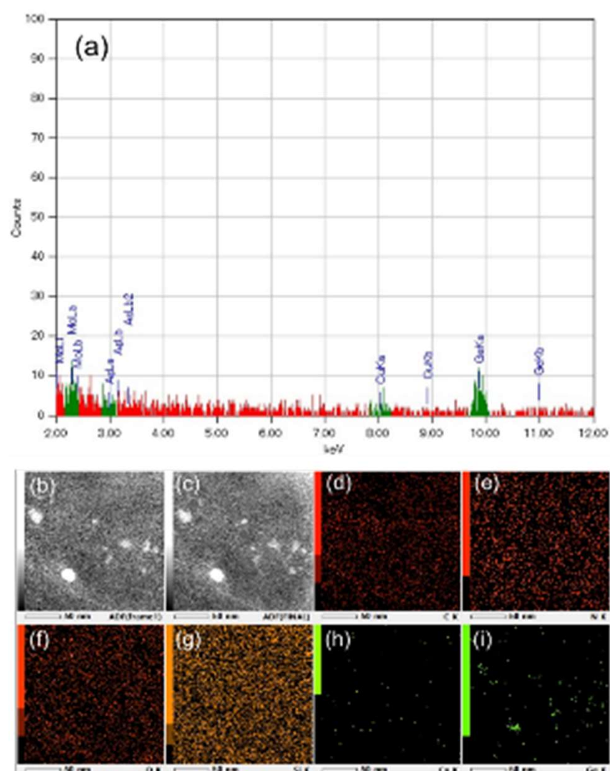

Figure 9. STEM-EDS obtained at RT after all annealing processes (after process #16). (a) EDS spectrum. (b,c) HAADF-STEM images (b) before and (c) after the EDS analysis. (d-i) EDS maps of (d) C, (e) N, (f) O, (g) Si, (h) Cu, and (i) Ge.

4. Nucleation and domain growth of Ge encapsulated by graphene layers

Figures 10(a-f) show the TEM images extracted from the *in situ* TEM movie for the process # 13 (S2 "growth"). The time and temperature are shown in the lower right corner of each TEM image. During the heating process, contrast changes were observed at various regions. Here, we focus on the circled region near the center of the TEM images. The contrast in the circled region remained dark during the temperature increase from RT to 1000 °C (Fig. 10(a-c)). Thereafter, the dark contrast faded while the temperature was kept constant at 1025 °C (Fig. 10(d) and 10(e)).

288 Figures 11(a-d) show magnified TEM image around the circled region in Fig. 10. The time and
289 temperature are shown in the upper left corner of each TEM image. At 750 °C during the temperature
290 increase, a tiny droplet Ge was observed (indicated by the arrow in Fig. 11(a)). When the temperature
291 reached 1025 °C, a new droplet Ge appeared (indicated by the left arrow in Fig. 11(b)). While the
292 temperature was maintained at 1025 °C, the size of the droplets Ge increased (Figs. 11(b-d)). At the same
293 time, the contrast in the circled broken line in Fig.11(a) gradually changed from dark to faint. The fading
294 contrast probably means that the condensed amorphous Ge diffused into the surroundings, resulting in
295 the reduction its concentration. These indicates that Ge crystal growth occurred and a Ge nucleus
296 incorporated the surrounding amorphous Ge. This situation is similar to the bulk crystal growth of Si and
297 Ge, such as Czochralski method,[20] and our TEM observations suggests that crystal growth of Ge between
298 graphene layers is possible. However, the crystal growth in this experiment (Fig. 11) seems to be three-
299 dimensional because the shape of the droplet Ge was spherical and no information about the two-
300 dimensionality could be obtained from the crystallized Ge. Therefore, more unique and new ideas are
301 needed to achieve the growth of 2D germanium (germanene) between vdW layers. For example, limiting
302 the direction of crystal growth by thinning the initial Ge source film to make it more truly 2D, or creating
303 a monolayer vdW/metal (111) heterostructure to induce remote epitaxy, as has been reported for graphene
304 growth on GaAs.[26]

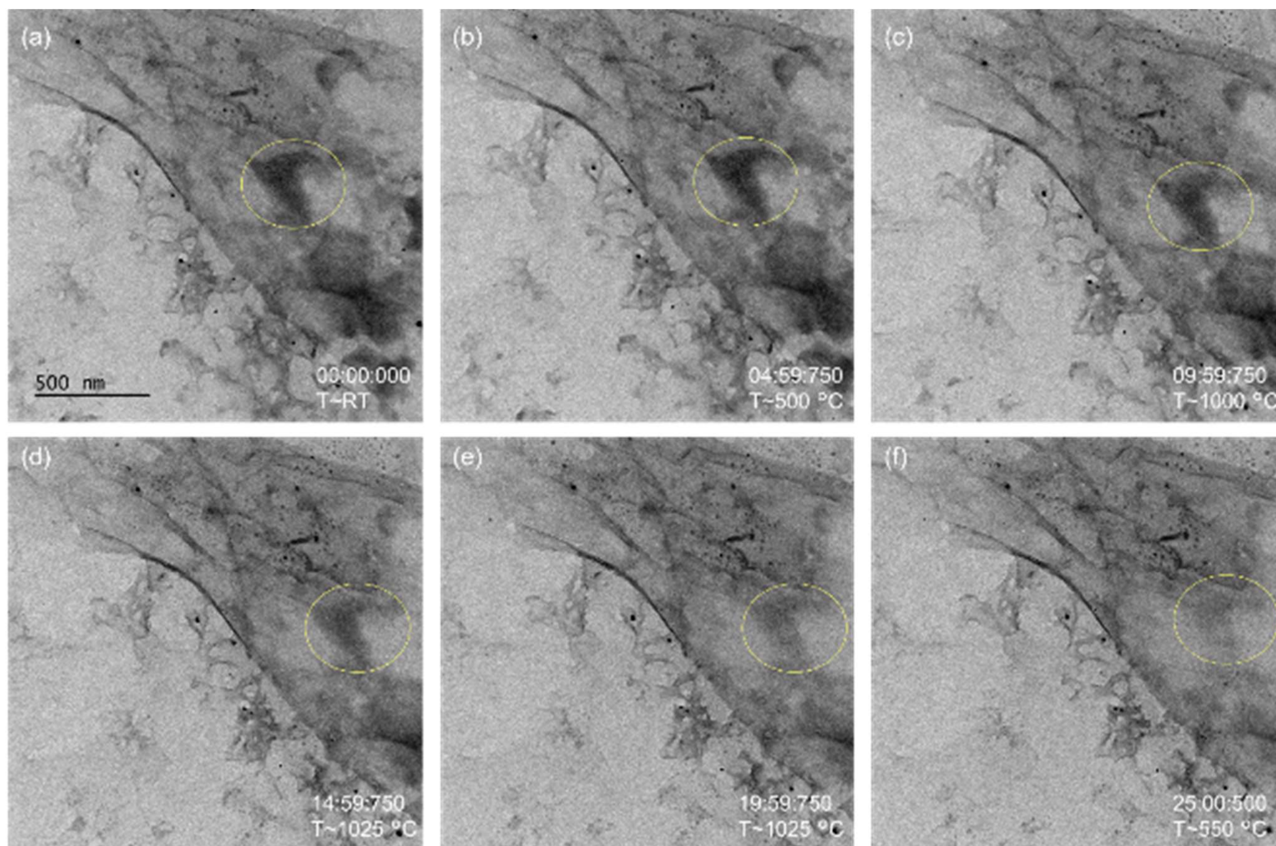

305

306 **Figure 10.** (a-f) TEM images extracted from the *in situ* TEM movie for the process #13. The time and

307 temperature are shown in the lower right corner of each TEM image.

308

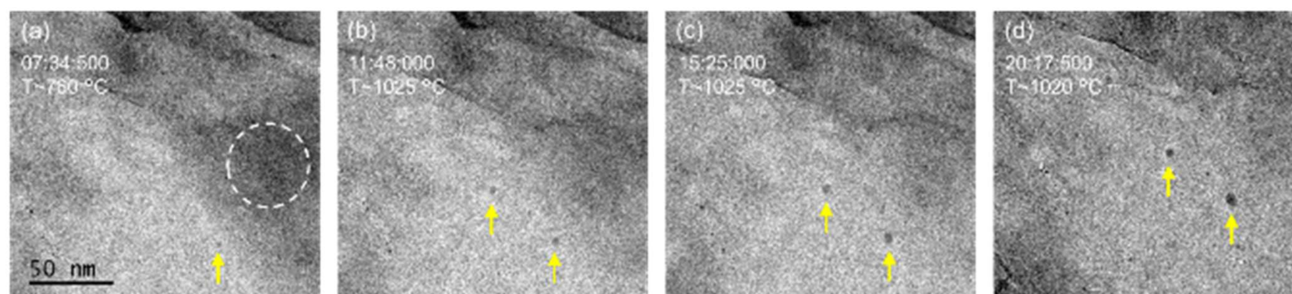

309

310 **Figure 11.** (a-d) Magnified TEM image around the circled region in Fig. 10. The time and temperature

311 are shown in the upper left corner of each TEM image. Ge droplets are indicated by arrows.

312

313 **Conclusion**

314 In this study, we fabricated a graphene/Ge/graphene encapsulated structure using transfer process of CVD
315 graphene. The fabricated encapsulated Ge was observed by *in situ* TEM to investigate how the Ge in the
316 vdW layer behaves at high temperatures, especially at temperatures higher than MP_{Ge}. The results showed
317 that graphene encapsulation played a role in suppressing Ge evaporation even above MP_{Ge}. At higher
318 temperatures than MP_{Ge}, the movement of Ge droplets and their coalescence with other Ge droplets in
319 the surrounding area were observed. *In situ* HRTEM observation at high temperatures revealed that some
320 droplets Ge do not have clear lattice fringes, indicating that Ge can exist as a liquid phase between vdW
321 layers. It was also observed that droplet Ge incorporates the surrounding amorphous Ge as Ge nuclei,
322 thereby increasing its domain size. These results indicate that the Ge encapsulation structure with vdW
323 materials can be used to grow Ge crystals, such like Czochralski method, between vdW layers. Although
324 more unique and new ideas will be needed to achieve the growth of germanene between vdW layers, the
325 present results may provide clues for the future direct growth of germanene between hBN layers.

326

327 **Methods**

328 CVD growth of graphene: CVD graphene was grown on a commercial Cu sheet (99.96% in purity, 100
329 µm thickness, Nilaco) in a homemade CVD system in NIMS. Polycrystalline monolayer graphene with
330 high coverage was targeted in the present CVD. The growth process was as follows: i) increasing the
331 temperature from RT to 800 °C in Ar; ii) increasing the temperature from 800 to 950 °C in H_2/Ar (~15%
332 H_2); iii) H_2/Ar (~10% H_2) annealing for 100 min at 1000 °C; iv) O_2/Ar (~20 ppm O_2) annealing for 35
333 min; v) graphene growth by introducing CH_4 (~50 ppm) with H_2 and Ar for 90 min; vi) additional

334 graphene growth in H_2/Ar and high concentrations of CH_4 (~0.1 %) for 5 min; vii) cooling to RT in H_2/Ar
335 (~2.5% H_2). The H_2/Ar and O_2/Ar annealing were performed to reduce nucleation density of graphene.[27]
336 The additional growth, so-called two-step growth,[28] was performed to increase the coverage of graphene.
337 The mechanisms related to this CVD growth are presented elsewhere.[27b, 27c, 29]

338 Transfer graphene: The transfer process (Fig. 1) basically follows the standard wet transfer process for
339 graphene.[30] PMMA was dissolved in anisole and then the suspension was spin-coated onto graphene/Cu.
340 $(NH_4)_2S_2O_8$ was used to etch Cu. To begin, Cu was etched for a short time (5-10 min). The sample was
341 taken out from the etchant and the backside graphene was removed by softly rubbing the backside of the
342 Cu with a commercially available cotton swab. After replacing the etchant with a new one, etching of Cu
343 restarted again. The short etching and rubbing were repeated twice in total, followed by the main etching
344 (usually several hours). After multiple DI rinses, the PMMA/graphene was then scooped up with another
345 graphene/Cu, and finally the PMMA layer was removed with acetone.

346 Ge deposition: Ge thin film of 20 nm thickness was deposited at RT by an e-beam evaporator (RDEC Co.,
347 with the Ltd., RDEB-1206K). The deposition rate was ~1.0 Å s^{-1}.

348 SEM-EDS: SEM and EDS analysis were performed using a commercial SEM (Hitachi TM4000).
349 Secondary electron images and EDS spectra were obtained at an acceleration voltage of 15 kV.

350 Raman spectroscopy: A commercial Raman microscope (Horiba, LabRam HR Evolution) with an
351 excitation wavelength of 458 nm was used for obtaining Raman spectra.

352 *In situ* heating TEM experiments: *In situ* TEM experiments on graphene-encapsulated Ge were conducted
353 using a DENSsolutions lightning sample holder in a spherical aberration (Cs)-corrected TEM, JEM-

354 ARM200F, operated at 200kV. OneView camera and drift correction were used. EDS mapping after a
355 heating process was performed after the sample temperature was cooled to RT.

356

357 **References**

358 [1] A. Acun, L. Zhang, P. Bampoulis, M. Farmanbar, A. van Houselt, A. Rudenko, M. Lingenfelder, G.
359 Brocks, B. Poelsema, M. Katsnelson, *J. Phys.: Condens. Matter* **2015**, 27, 443002.

360 [2] S. Cahangirov, M. Topsakal, E. Aktürk, H. Şahin, S. Ciraci, *Phys. Rev. Lett.* **2009**, 102, 236804.

361 [3] Z. Ni, Q. Liu, K. Tang, J. Zheng, J. Zhou, R. Qin, Z. Gao, D. Yu, J. Lu, *Nano Lett.* **2011**, 12, 113.

362 [4] M. Ezawa, *J. Phys. Soc. Jpn.* **2015**, 84, 121003.

363 [5] G. Fiori, F. Bonaccorso, G. Iannaccone, T. Palacios, D. Neumaier, A. Seabaugh, S. K. Banerjee, L.
364 Colombo, *Nat. Nanotechnol.* **2014**, 9, 768.

365 [6] P. Vogt, P. De Padova, C. Quaresima, J. Avila, E. Frantzeskakis, M. C. Asensio, A. Resta, B. Ealet,
366 G. Le Lay, *Phys. Rev. Lett.* **2012**, 108, 155501.

367 [7] a) J. Yuhara, Y. Fujii, K. Nishino, N. Isobe, M. Nakatake, L. Xian, A. Rubio, G. Le Lay, *2D Mater.*
368 **2018**, 5, 025002; b) F.-f. Zhu, W.-j. Chen, Y. Xu, C.-l. Gao, D.-d. Guan, C.-h. Liu, D. Qian, S.-C.
369 Zhang, J.-f. Jia, *Nat. Mater.* **2015**, 14, 1020; c) Y. Xu, B. Yan, H.-J. Zhang, J. Wang, G. Xu, P. Tang,
370 W. Duan, S.-C. Zhang, *Phys. Rev. Lett.* **2013**, 111, 136804.

371 [8] J. Yuhara, B. He, N. Matsunami, M. Nakatake, G. Le Lay, *Adv. Mater.* **2019**, 31, 1901017.

372 [9] a) S. Suzuki, T. Iwasaki, K. K. H. De Silva, S. Suehara, K. Watanabe, T. Taniguchi, S. Moriyama,
373 M. Yoshimura, T. Aizawa, T. Nakayama, *Adv. Funct. Mater.* **2021**, 31, 2007038; b) L. Kesper, J. A.
374 Hochhaus, M. Schmitz, M. G. Schulte, U. Berges, C. Westphal, *Sci. Rep.* **2022**, 12, 1; c) J. Yuhara,
375 H. Shimazu, K. Ito, A. Ohta, M. Araidai, M. Kurosawa, M. Nakatake, G. Le Lay, *ACS Nano* **2018**,
376 12, 11632; d) C.-H. Lin, A. Huang, W. W. Pai, W.-C. Chen, T.-Y. Chen, T.-R. Chang, R. Yukawa, C.-

377 M. Cheng, C.-Y. Mou, I. Matsuda, C. T. C., J. H. T., T. S. J., *Phys. Rev. Mater.* **2018**, 2, 024003; e)
378 A. Ohta, K. Yamada, H. Sugawa, N. Taoka, M. Ikeda, K. Makihara, S. Miyazaki, *Jpn. J. Appl. Phys.*
379 **2021**, 60, SBBK05; f) S. Suzuki, K. K. H. De Silva, M. Yoshimura, T. Nakayama, *Jpn. J. Appl. Phys.*
380 **2020**, 59, SN1004; g) K. Ito, A. Ohta, M. Kurosawa, M. Araidai, M. Ikeda, K. Makihara, S. Miyazaki,
381 *Jpn. J. Appl. Phys.* **2018**, 57, 06HD08.
382 [10] a) M. Dávila, L. Xian, S. Cahangirov, A. Rubio, G. Le Lay, *NJPh* **2014**, 16, 095002; b) M. E. Dávila,
383 G. Le Lay, *Sci. Rep.* **2016**, 6, 20714.
384 [11] Z. Qin, J. Pan, S. Lu, Y. Shao, Y. Wang, S. Du, H. J. Gao, G. Cao, *Adv. Mater.* **2017**, 29, 1606046.
385 [12] a) Y. Sato, Y. Fukaya, M. Cameau, A. K. Kundu, D. Shiga, R. Yukawa, K. Horiba, C.-H. Chen, A.
386 Huang, H.-T. Jeng, T. Ozaki, H. Kumigashira, M. Niibe, I. Matsuda, *Phys. Rev. Mater.* **2020**, 4,
387 064005; b) J. Yuhara, H. Muto, M. Araidai, M. Kobayashi, A. Ohta, S. Miyazaki, S.-i. Takakura, M.
388 Nakatake, G. Le Lay, *2D Mater.* **2021**, 8, 045039; c) M. Derivaz, D. Dentel, R. Stephan, M.-C. Hanf,
389 A. Mehdaoui, P. Sonnet, C. Pirri, *Nano Lett.* **2015**, 15, 2510; d) S. Endo, O. Kubo, N. Nakashima,
390 S. Iwaguma, R. Yamamoto, Y. Kamakura, H. Tabata, M. Katayama, *Appl. Phys. Express* **2017**, 11,
391 015502; e) O. Kubo, S. Kinoshita, H. Sato, K. Miyamoto, R. Sugahara, S. Endo, H. Tabata, T. Okuda,
392 M. Katayama, *Phys. Rev. B* **2021**, 104, 085404; f) M. Kobayashi, A. Ohta, M. Kurosawa, M. Araidai,
393 N. Taoka, T. Simizu, M. Ikeda, K. Makihara, S. Miyazaki, *Jpn. J. Appl. Phys.* **2020**, 59, SGGK15.
394 [13] L. Li, S. z. Lu, J. Pan, Z. Qin, Y. q. Wang, Y. Wang, G. y. Cao, S. Du, H. J. Gao, *Adv. Mater.* **2014**,
395 26, 4820.
396 [14] L. Persichetti, F. Jardali, H. Vach, A. Sgarlata, I. Berbezier, M. De Crescenzi, A. Balzarotti, *J. Phys.*
397 *Chem.* **2016**, 7, 3246.
398 [15] a) L. Zhang, P. Bampoulis, A. Rudenko, Q. v. Yao, A. Van Houselt, B. Poelsema, M. Katsnelson, H.
399 Zandvliet, *Phys. Rev. Lett.* **2016**, 116, 256804; b) Z. Jiao, Q. Yao, A. Rudenko, L. Zhang, H.
400 Zandvliet, *Phys. Rev. B* **2020**, 102, 205419.

401 [16] a) B. Madhushankar, A. Kaverzin, T. Giousis, G. Potsi, D. Gournis, P. Rudolf, G. Blake, C. Van Der
402 Wal, B. Van Wees, *2D Mater.* **2017**, 4, 021009; b) Q. Chen, L. Liang, G. Potsi, P. Wan, J. Lu, T.
403 Giousis, E. Thomou, D. Gournis, P. Rudolf, J. Ye, *Nano Lett.* **2019**, 19, 1520; c) Y. Katayama, R.
404 Yamauchi, Y. Yasutake, S. Fukatsu, K. Ueno, *Appl. Phys. Lett.* **2019**, 115, 122101.
405 [17] L. Tao, E. Cinquanta, D. Chiappe, C. Grazianetti, M. Fanciulli, M. Dubey, A. Molle, D. Akinwande,
406 *Nat. Nanotechnol.* **2015**, 10, 227.
407 [18] a) C. R. Dean, A. F. Young, I. Meric, C. Lee, L. Wang, S. Sorgenfrei, K. Watanabe, T. Taniguchi, P.
408 Kim, K. L. Shepard, J. Hone, *Nat. Nanotechnol.* **2010**, 5, 722; b) J. Xue, J. Sanchez-Yamagishi, D.
409 Bulmash, P. Jacquod, A. Deshpande, K. Watanabe, T. Taniguchi, P. Jarillo-Herrero, B. J. LeRoy, *Nat.*
410 *Mater.* **2011**, 10, 282; c) L. Banszerus, M. Schmitz, S. Engels, J. Dauber, M. Oellers, F. Haupt, K.
411 Watanabe, T. Taniguchi, B. Beschoten, C. Stampfer, *Sci. Adv.* **2015**, 1, e1500222; d) T. Iwasaki, Y.
412 Morita, K. Watanabe, T. Taniguchi, *Phys. Rev. B* **2022**, 106, 165134; e) T. Iwasaki, S. Nakaharai, Y.
413 Wakayama, K. Watanabe, T. Taniguchi, Y. Morita, S. Moriyama, *Nano Lett.* **2020**, 20, 2551.
414 [19] a) M. Y. Chan, K. Komatsu, S.-L. Li, Y. Xu, P. Darmawan, H. Kuramochi, S. Nakaharai, A.
415 Aparecido-Ferreira, K. Watanabe, T. Taniguchi, K. Tsukagoshi, *Nanoscale* **2013**, 5, 9572; b) G. H.
416 Lee, Y. J. Yu, X. Cui, N. Petrone, C. H. Lee, M. S. Choi, D. Y. Lee, C. Lee, W. J. Yoo, K. Watanabe,
417 T. Taniguchi, C. Nuckolls, P. Kim, J. Hone, *ACS Nano* **2013**, 7, 7931; c) Y. Shimazaki, I. Schwartz,
418 K. Watanabe, T. Taniguchi, M. Kroner, A. Imamoğlu, *Nature* **2020**, 580, 472.
419 [20] a) G. K. Teal, M. Sparks, E. Buehler, *Phys. Rev.* **1951**, 81, 637; b) G. K. Teal, J. B. Little, *Phys. Rev.*
420 **1950**, 78, 647.
421 [21] a) P. Germain, K. Zellama, S. Squelard, J. Bourgoin, A. Gheorghiu, *J. Appl. Phys.* **1979**, 50, 6986;
422 b) N. A. Blum, C. Feldman, *J. Non-Cryst. Solids* **1976**, 22, 29; c) K. Chik, P.-K. Lim, *Thin Solid*
423 *Films* **1976**, 35, 45.

424 [22] a) A. C. Ferrari, J. Robertson, *Philosophical Transactions of the Royal Society of London A: Mathematical, Physical and Engineering Sciences* **2004**, 362, 2477; b) L. Malard, M. Pimenta, G. Dresselhaus, M. Dresselhaus, *PhR* **2009**, 473, 51; c) A. Ferrari, J. Meyer, V. Scardaci, C. Casiraghi, M. Lazzeri, F. Mauri, S. Piscanec, D. Jiang, K. Novoselov, S. Roth, *Phys. Rev. Lett.* **2006**, 97, 187401.

428 [23] a) M. M. Treacy, *Microscopy and Microanalysis* **2011**, 17, 847; b) N. Tanaka, *Scanning transmission electron microscopy of nanomaterials: basics of imaging and analysis*, World Scientific, **2014**.

430 [24] a) L. C. Kelsall, M. Peña-Alvarez, M. Martinez-Canales, J. Binns, C. J. Pickard, P. Dalladay-Simpson, R. T. Howie, E. Gregoryanz, *The Journal of Chemical Physics* **2021**, 154, 174702; b) H. Weis, D. Holland-Moritz, F. Kargl, F. Yang, T. Unruh, T. Hansen, J. Bednarčik, A. Meyer, *Phys. Rev. B* **2021**, 104, 134108; c) I. Pozdnyakova, O. Roik, J. W. Drewitt, A. Bytchkov, F. Kargl, S. Jahn, S. Brassamin, L. Hennet, *J. Phys.: Condens. Matter* **2021**, 33, 244002; d) Y. Naito, M. Inui, T. Anai, K. Tamura, *J. Non-Cryst. Solids* **2007**, 353, 3376; e) G. Kresse, J. Hafner, *Phys. Rev. B* **1994**, 49, 14251; f) N. Ashcroft, *Il Nuovo Cimento D* **1990**, 12, 597.

437 [25] H. Weis, F. Kargl, M. Kolbe, M. Koza, T. Unruh, A. Meyer, *J. Phys.: Condens. Matter* **2019**, 31, 455101.

439 [26] Y. Kim, S. S. Cruz, K. Lee, B. O. Alawode, C. Choi, Y. Song, J. M. Johnson, C. Heidelberger, W. Kong, S. Choi, *Nature* **2017**, 544, 340.

441 [27] a) I. Vlassiouk, M. Regmi, P. Fulvio, S. Dai, P. Datskos, G. Eres, S. Smirnov, *ACS nano* **2011**, 5, 6069; b) S. Suzuki, K. Kiyosumi, T. Nagamori, K. Tanaka, M. Yoshimura, *e-J. Surf. Sci. Nanotechnol.* **2015**, 13, 404; c) S. Suzuki, Y. Terada, M. Yoshimura, *Coatings* **2017**, 7, 206.

444 [28] X. Li, C. W. Magnuson, A. Venugopal, J. An, J. W. Suk, B. Han, M. Borysiak, W. Cai, A. Velamakanni, Y. Zhu, L. Fu, E. M. Vogel, E. Voelkl, L. Colombo, R. S. Ruoff, *Nano Lett.* **2010**, 10, 4328.

447 [29] Y. Hao, M. S. Bharathi, L. Wang, Y. Liu, H. Chen, S. Nie, X. Wang, H. Chou, C. Tan, B. Fallahazad,
448 H. Ramanarayan, C. W. Magnuson, E. Tutuc, B. I. Yakobson, K. F. McCarty, Y. W. Zhang, P. Kim,
449 J. Hone, L. Colombo, R. S. Ruoff, *Science* **2013**, 342, 720.
450 [30] a) X. Li, Y. Zhu, W. Cai, M. Borysiak, B. Han, D. Chen, R. D. Piner, L. Colombo, R. S. Ruoff, *Nano*
451 *Lett.* **2009**, 9, 4359; b) H. J. Jeong, H. Y. Kim, S. Y. Jeong, J. T. Han, K.-J. Baeg, J. Y. Hwang, G.-
452 W. Lee, *Carbon* **2014**, 66, 612; c) S. Suzuki, M. Yoshimura, *Sci. Rep.* **2017**, 7, 14851.
453 **Acknowledgements**
454 This study was supported in part by JSPS KAKENHI Grant number 20K15134 (Grant-in-Aid for
455 Early-Career Scientists) from the Ministry of Education, Culture, Sports, Science and Technology
456 (MEXT), Japan; Japan Science and Technology Agency (JST), Precursory Research for Embryonic
457 Science and Technology (PRESTO) Grant Number JPMJPR21B7; NIMS Nanofabrication Platform
458 supported by "Nanotechnology Platform Program" of the MEXT, Grant Number JPMXP09F19NMN010;
459 Materials Analysis Station in NIMS; NIMS Electron Microscopy Analysis Station, Nanostructural
460 Characterization Group; the Public/Private R&D Investment Strategic Expansion Program (PRISM) from
461 Cabinet Office, Japan; the Center for Functional Sensor and Actuator (CFSN) from NIMS.

462

463 **Author contributions statement**
464 S.S. designed the research. S.S. and N.S. conducted sample preparation, SEM-EDS, and Raman
465 spectroscopy. Y.Ne. conducted TEM observation. S.S., N.S., Y.Na, and Y.Ne discussed many times to
466 improve the sample preparation and TEM observation. S.S. and Y.Ne analyzed the results. S.S., Y.Ne.,
467 Y.Na and M.T. discussed interpretation of the results. S.S. mainly wrote the manuscript. All authors
468 reviewed the manuscript.

469

470 **Conflict of Interest**

471 The authors declare no conflict of interest.

472

473 **Keywords**

474 germanene, germanium, graphene, van der Waals materials, interface, crystal growth, nucleation,
475 transmission electron microscopy, graphene cell for transmission electron microscopy, high-angle annular
476 dark field scanning transmission electron microscopy, *in situ* heating measurement